Chapter 6

Analysis and Control of Ultrafast Processes in $CpMn(CO)_3$

Organometallic compounds containing transition metals as well as CO ligands are adequate systems for investigating the dynamics of unimolecular photo-dissociation passages, in particular those which occur on electronic excited states. The chromophore character of their metallic core allows irradiation with femtosecond laser pulses. Moreover their dissociative tendency is an important feature which can be exploited in optimal control of different fragmentation branches.

This chapter starts with a short description of the chosen molecule cyclopentadienyl manganese tricarbonyl (cymantrene), $CpMn(CO)_3$, for the real-time studies with femtosecond laser pulses. Previous work of other researchers on a few organometallic systems is briefly mentioned as well. Mass-spectrometric studies are performed at different wavelengths and laser pulse peak intensity. The recorded mass spectra show the production of different photo-fragments as a function of these laser parameters.

The two-color pump–probe experiments are described in the following section. It will be shown that the femtosecond studies lead to the understanding of the optimal pulse obtained in a previous experiment for controlling the ionization process of the parent molecule. The ionization of $CpMn(CO)_3^+$ was optimized in an adaptive feedback loop by applying an evolutionary algorithm. The experimental work together with theoretical simulations of the involved dynamics on electronic excited states allowed the deciphering of the mechanism of the optimized process. The section ends with the description of a pump–probe experiment in which the peak intensity of the pump pulse is changed by a factor of four.

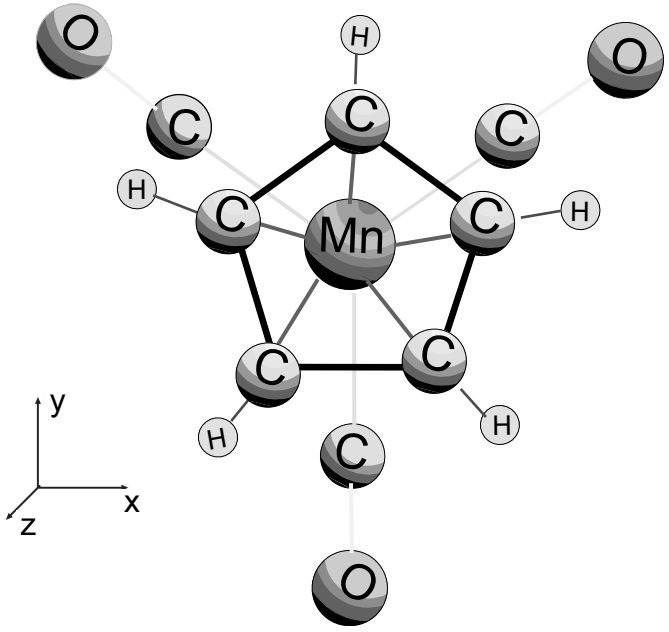

Figure 6.1: A topview of the structure of the cyclopentadienyl manganese tricarbonyl ($CpMn(CO)_3$) after Ref. [119]. For a C_s symmetry the mirror plane is the *yz*-plane.

Optimal control studies on the first fragment ion, $CpMn(CO)_2$, are described in the last section.

6.1 Choice of the System

The structure of $CpMn(CO)_3$, according to Ref. [119], is shown in Figure 6.1. The central manganese atom is bound to a cyclopentadienyl group and to three CO ligands. The molecule has a C_s symmetry at the low temperatures of the molecular beam. The ionization potential of the molecule is about 7.26 eV [120].

The calculated potential energy surfaces as a function of the Mn–CO coordinate are shown in Figure 6.2. The involved electronic states are the following: the electronic ground state a^1A', the excited states a^1A'', b^1A', c^1A', b^1A'' and the ionic states $(a^2A'')^+$, $(a^2A')^+$, $(b^2A')^+$. For a C_s symmetry, which corresponds to the low temperatures of the molecular beam the mirror plane is the *yz* direction. Thus the selection rules for the excitation step are: (i) the A' states can be excited only by *y* or *z* polarized light and (ii) the A'' states can be excited only by *x* polarized light [120]. Other combinations are not allowed due to symmetry reasons. Therefore in a pump–probe experiment

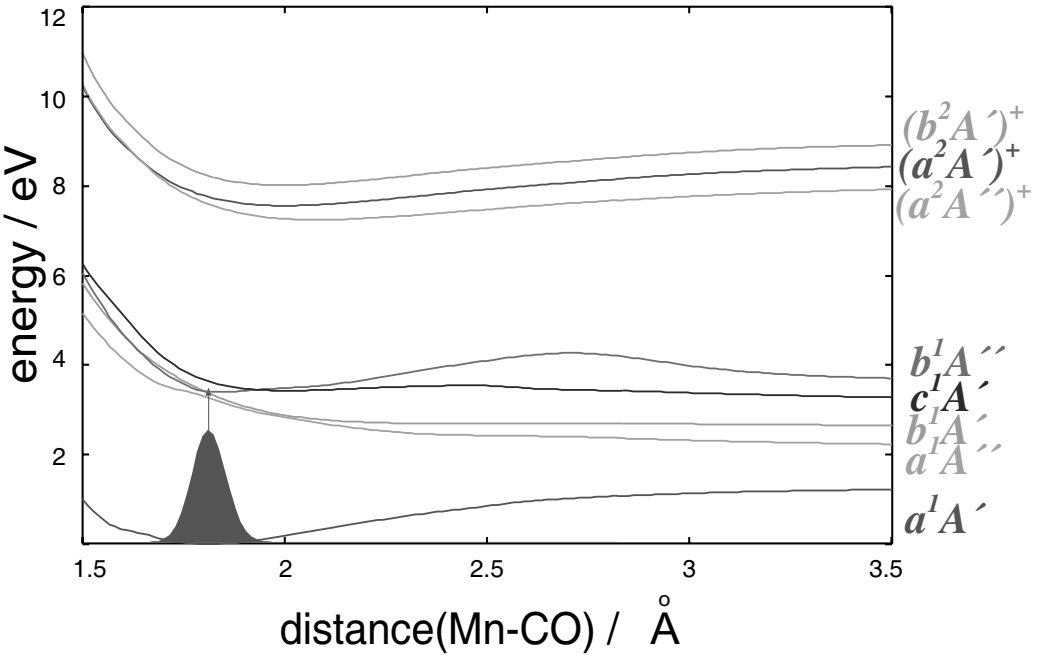

Figure 6.2: Potential energy surfaces of cyclopentadienyl manganese tricarbonyl ($CpMn(CO)_3$) as a function of Mn–CO coordinate [121]. The arrow indicates an excitation step from the ground state a^1A' into the involved electronic excited states.

the electric fields of the two pulses should have orthogonal polarization with respect to each other.

Many groups have performed femtosecond experiments on organometallic complexes. This allowed the investigation of molecular dynamics in real-time by means of pump–probe technique [122–126] and in some cases control of ultrafast processes [108, 127].

Trushin and co-workers have studied the consecutive photo-dissociation channels of many organometallic compounds including $M(CO)_6$, M = Cr, Mo, W [122] and $Fe(CO)_5$ [123] by employing the femtosecond pump–probe spectroscopy. After excitation, if probed through the ionization window, the first observable is the $M(CO)_n^+$ parent molecule, followed by its primary photoproduct $M(CO)_{n-1}^+$. Then, the next fragment ion $M(CO)_{n-2}^+$, appears etc., until the naked metal is reached. They have investigated the fragmentation patterns in 1,3-cyclohexadiene, as well, which depend on the locations of the wave packet on potential energy surfaces [124]. By monitoring different fragment ions, their method allowed the interrogation of the population at these locations.

Zewail and co-workers [125] have examined the femtosecond dynamics of

the metal-metal and metal-ligand bond cleavage in the $Mn_2(CO)_{10}$ molecule and resolved two main fragmentation channels: first, when the molecule loses one CO ligand, and second, when the Mn-Mn bond is broken and the molecule is split in two $Mn(CO)_5$ fragments.

Bañarez and co-workers [126] have reported a fast photo-fragmentation study on the $Fe(CO)_5$ compound. The electronically excited molecule loses 4 CO ligands within 100 fs; the last CO ligand is lost after approximately 230 fs. They found that the $Fe(CO)_n$ (n = 2,3,4) fragments have the same fingerprints, reflecting the evolution of the $[Fe(CO)_5]^{\ddagger}$ transition state on its way to the fragmentation channel(s).

The pronounced fragmentation inclination of these species clearly demonstrate that organometallic compounds containing CO ligands are eligible candidates for controlling their molecular dynamics in real-time. The manipulation of reaction dynamics by driving the molecule towards a desired target can be achieved, for example by combining the idea of Judson and Rabitz [5] of using a self-learning algorithm (see Chapter 5 section 5.2.4) with Weiner's proposed pulse shaping technique [4].

The major goal of our adaptive control experiments is not only to drive reaction dynamics, but to gain information about the photo-induced control process itself from the acquired optimal laser field [109]. This observable is suitable for this inversion problem [6], because the optimal pulse shape should in principle reflect information about the propagation processes of the created wave packets on the involved potential energy surfaces (PES).

Therefore the previous studies performed in our group [59, 127–129] focused on inquiring the fragmentation processes occurring in $CpMn(CO)_3$. First experimental results were obtained and presented in Ref. [59]. For example, after being ionized by an electron gun, the recorded mass spectra reflect fragmentation patterns, strongly depending on the electron impact energy. Using 87 fs laser pulses centered at 800 nm, the mass spectra reflected a strong dependence on the pulse energy. When employing linearly downchirped pulses, an increase of the CpMn(CO) ion intensity of 100 % relative to the mother molecule was observed [129].

6.2 Experimental Preparations

The experimental layout used for the analysis of ultrafast processes in $CpMn(CO)_3$ is displayed in Figure 6.3.

The molecular beam apparatus is described in Chapter 4, section 4.1.1. In the preparation chamber yellow $CpMn(CO)_3$ crystals filled half of a TZM skiff. The 2 g of the sample are heated up to 75 °C in the stainless steel

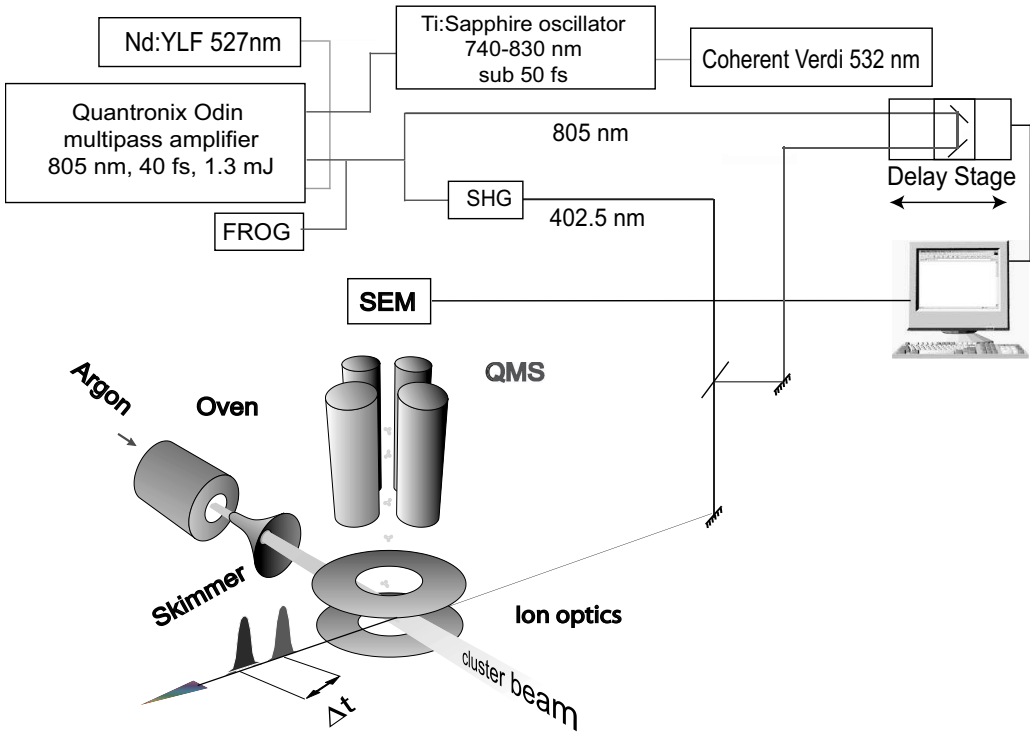

Figure 6.3: The experimental apparatus used in femtosecond investigations of $CpMn(CO)_3$. The laser system (FS II, see Chapter 4, section 4.2.2) is depicted in the upper part, whereas in the lower part the molecular beam apparatus is schematically presented. In the pump–probe experiments, the emerging amplified pulses are directed to a Mach-Zhender-type interferometer, where an arm is frequency-doubled. The mass spectrometric studies are done with a single pulse. The $CpMn(CO)_3$ neutral molecules are prepared in a molecular beam. Details are given in the text.

cartridge assuring a continuous molecular beam for about 50 hours by co-expanding the $CpMn(CO)_3$ sample vapor with 0.2-0.4 mbar of argon across a 90 μm nozzle into the vacuum. The argon flow is set at 15-17 standard cubic centimeters per minute. The beam containing cold molecules enters the interaction chamber after passing through a 2 mm skimmer. The interaction chamber is differentially pumped by the two turbo molecular pumps allowing a 5 x 10^{-6} mbar pressure during the measurements. The laser pulses intersect the molecular beam passing between the electrical lenses of the quadrupole mass spectrometer. The resulting photo-ions are mass-selected with a resolution m/Δm better than 200. The ion current is measured by the secondary electron multiplier and then further amplified.

The employed laser system (FS II) is described in Chapter 4, section 4.2.2. Briefly, it consists of the tunable Ti:sapphire oscillator (Kapteyn-Murnane) pumped by a Coherent Verdi V5. The oscillator is used to seed the multipass amplifier (Quantronix, Odin) in order to obtain 40 fs pulses of 1.3 mJ energy at 805 nm central wavelength and 1 kHz repetition rate.

After the amplification and compression, the laser pulses are split up in two: the first pulse (pump) is frequency-doubled in a 0.3 mm BBO crystal, aligned at the optimal phase-matching angle. The second pulse (probe) is send through a computer-motorized optical delay stage. The two pulses are then recombined in a Mach-Zhender-type arrangement and focused on the cluster beam by a 25 mm achromatic lens. The laser pulses were analyzed with the SHG FROG technique [22]. In this way pump–probe experiments can be performed. Mass spectra can be recorded by using single laser pulses at different laser intensities and central wavelengths. The laser pulses irradiate the molecular beam through a low-dispersion quartz window. The time-resolved mass spectra are measured with two pulses by changing the time delay between the pump and the probe pulses. The time zero between the 402.5 nm pump pulses and 805 nm probe pulses in the irradiation area is found with two methods: by generating sum-frequency in a 0.2 mm THG BBO type II crystal and by recording a transient spectrum of the ionized carrier gas.

6.3 Femtosecond Analysis of Ultrafast Processes in $CpMn(CO)_3^+$

This section contains femtosecond investigations of the ultrafast phenomena occurring in $CpMn(CO)_3^+$. First, mass spectra are recorded at different central laser wavelengths and peak intensities in order to monitor the production and identification of the photo-fragments. These studies give insights into the fragmentation process occurring on electronic excited states at the employed wavelengths and intensities. Moreover time-resolved mass spectra recorded with two laser pulses are expected to reveal information about the time scale on which dissociation of parent molecule takes place. The next section of the chapter focuses on two-color pump–probe experiments. Preliminary measurements with longer pulses from which the dissociation behavior of the parent ion and its fragment ions are discussed. The following section describes the pump–probe experiments performed with shorter pulses at slightly different central wavelengths. The observed wave packet dynamics helps deciphering the ionization mechanism performed by the optimal pulse

obtained for maximization of the $CpMn(CO)_3^+$ ion yield. The last section shows the pump–probe traces recorded at a higher pump photon intensity. These experiments confirm again the sensitivity of the studied system ions on the laser peak intensity.

6.3.1 Mass-spectrometric Studies

This section describes in the first part the mass spectra recorded with single femtosecond laser pulses of 45 fs duration at 402.5 nm and with 35 fs pulses centered at 805 nm, respectively. The evolution of the fragmentation degree as a function of laser peak intensity is presented as well. In the last part of this section time-resolved mass spectra recorded with two pulses centered around the aforementioned wavelengths are presented. They try to inquire on which temporal scale the fragmentation of $CpMn(CO)_3^+$ parent molecule occurs.

Mass Spectrometry at 402.5 nm

Figure 6.4 shows a set of mass spectra measured at 402.5 nm at different pulse peak intensities by employing 45 fs laser pulses. The laser intensity is tuned between 42 and 102 GW cm^{-2}. The z-axis represents the absolute value obtained by integration of every mass peak. The following masses are assigned to the corresponding ions: 55 a.m.u. (Mn^+), 120 a.m.u. ($CpMn^+$), 148 a.m.u. ($CpMn(CO)^+$), 176 a.m.u. ($CpMn(CO)_2^+$) and 204 a.m.u. ($CpMn(CO)_3^+$).

As it can be seen from Figure 6.4 the investigated system has a pronounced fragmentation tendency. The increase of the laser intensity changes the distribution of the emerging fragment ions. At higher pulse intensities relatively more Mn^+ and $CpMn^+$ are produced than $CpMn(CO)^+$ and $CpMn(CO)_2^+$.

Mass Spectrometry at 805 nm

Furthermore, mass spectra are recorded by employing 35 fs laser pulses centered at 805 nm. The dependence of the mother ion signal $CpMn(CO)_3^+$ together with its fragment ions on the laser intensity is depicted in Figure 6.5. The previously observed species at 402.5 nm are easily distinguishable at 805 nm as well. The increase of the laser peak intensity between 11 and 29 GW cm^{-2} mainly leads to an increase of intensity of the mother ion. This can be observed also in Figure 6.6, where only the dependence of ion yield of the parent molecule on the employed peak intensity over a larger interval was plotted. The increase of the ion signal with the laser intensity shows a

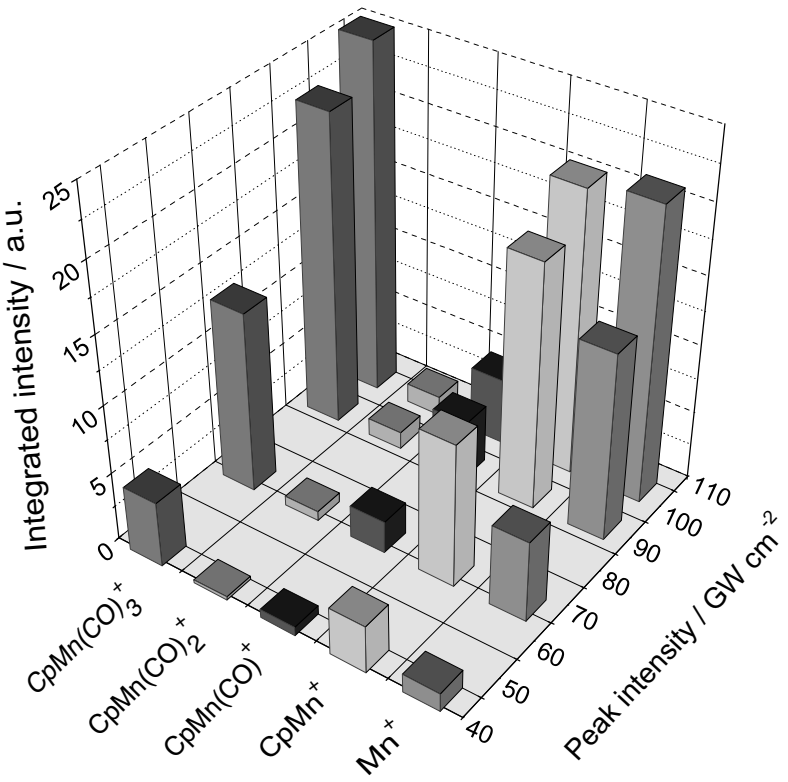

Figure 6.4: Set of mass spectra recorded with a single laser pulse of 45 fs time duration (at FWHM) centered around 402.5 nm [130]. The columns represent the absolute intensity integrated for each mass peak. The laser pulse peak intensity is varied between 42 and 102 GW cm^{-2}.

quadratic dependence. The intensities of the fragment peaks are very low in comparison with the spectrum recorded at 402.5 nm, but they increase as well.

The mass-spectroscopy spectra recorded at 402.5 nm and 805 nm, respectively, reveal the sensitivity of molecular system under the laser wavelength and peak intensity. However, this is a general, quite expected result. An insight in the dissociation phenomenon can be gained by investigating the degree of fragmentation as a function of laser intensity.

The Fragmentation Degree

Figure 6.7 shows the degree of fragmentation as a function of the laser pulse peak intensity. The degree of fragmentation represents the ratio between the sum of the integrated intensities of all fragments and the integrated intensity of the parent ion ($I_{fragments}$ / I_{parent}).

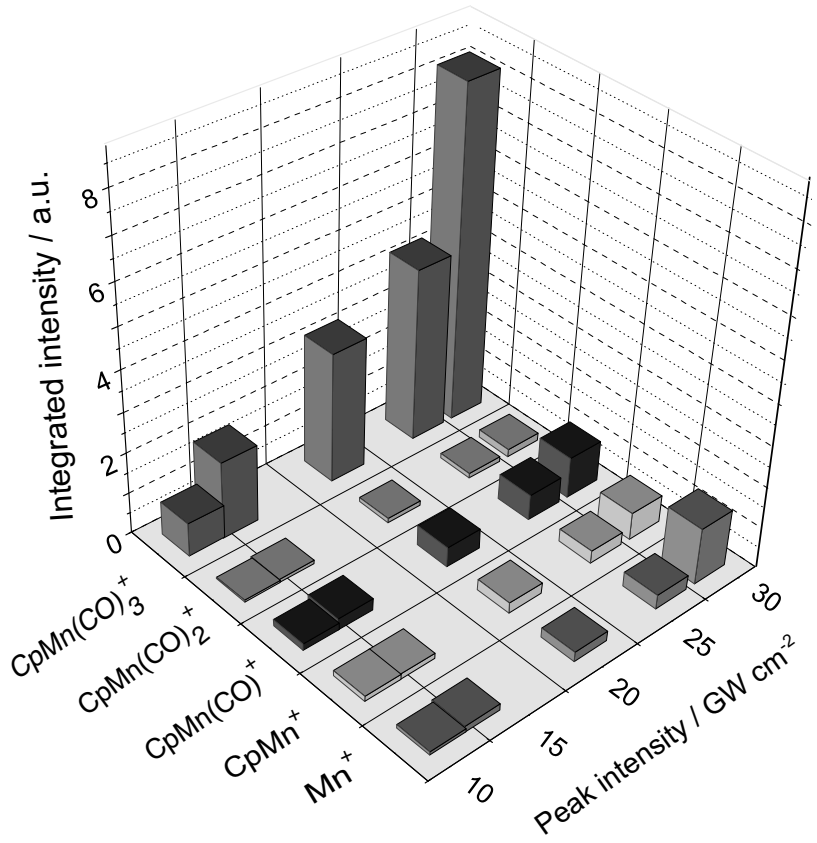

Figure 6.5: Set of mass spectra recorded with a single pulse of 35 fs at FWHM centered around 805 nm [130]. The columns represent the absolute intensity integrated for each mass peak. The laser pulse peak intensity is tuned between 11 and 29 GW cm^{-2}.

At 402.5 nm (3.07 eV) the ratio $I_{fragments}$ / I_{parent} increases with the irradiated intensity (Figure 6.7a). The parent ion absorbs three photons of 3.07 eV for the ionization (1.95 eV above the ionization threshold). The more energy is given to the system, the higher the fragmentation degree of the parent ion. This could give hints about dissociative excited states resonant or close to the resonance with 402.5 nm. It can not be excluded that the fragmentation at 402.5 nm occurs in the ion as well, since the extra energy given to the molecule after a three-photon process is much higher than the ionization energy. The increase of the ratio $I_{fragments}$ / I_{parent} with increasing laser intensity is a frequently expected phenomenon, observed also by other groups [131].

In Figure 6.7b the degree of fragmentation as a function of the peak intensity at 805 nm central wavelength is shown. The laser intensity is tuned

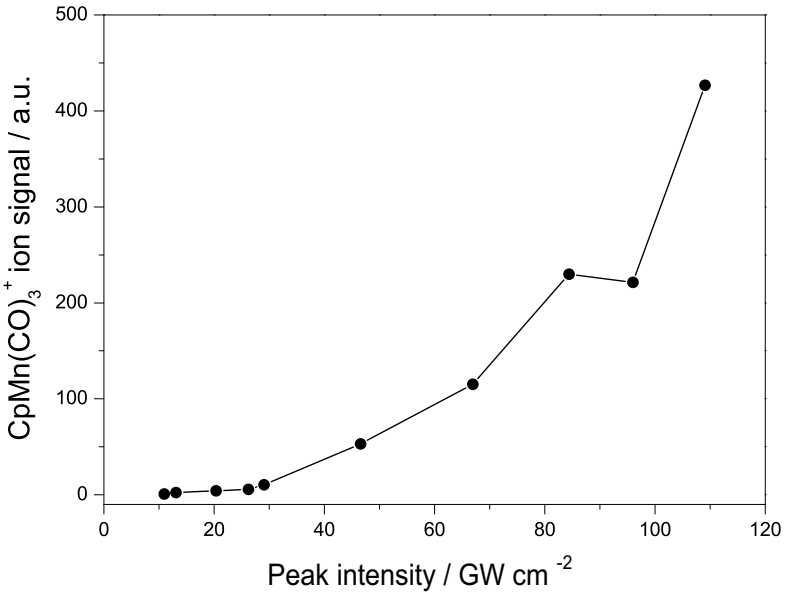

Figure 6.6: The ion signal distribution of the parent ion $CpMn(CO)_3^+$ as a function of laser pulse peak intensity. The wavelength was set at 805 nm.

from 11 GW cm^{-2} to 96 GW cm^{-2}. At low intensities, of up to 69 GW cm^{-2}, an interesting phenomenon is observed. The more energy is given to the molecule, the less effective is the $CpMn(CO)_3^+$ dissociation. The degree of fragmentation decreases until 69 GW cm^{-2} and increases for higher peak intensities employed. For ionizing the parent molecule with a single pulse at 805 nm (1.53 eV), the molecule has to absorb 5 photons of each 1.53 eV energy. This corresponds to an excess energy given to the system of only 0.39 eV.

The dependence of the fragmentation degree displayed in Figure 6.7b was observed also by other researchers for $Ni(CO)_4$ compound at low laser intensities [131]. They suggest that at low intensities, the ionization process follows relaxation. Thus it is expected that relaxation occurs in an electronic excited state (in our case pumped by two 805 nm photons). At higher peak intensities ionic fragmentation may occur. Furthermore, according to their study, the degree of fragmentation should not change with the pulse duration. In this work this feature is not observed because the employed pulse durations are kept constant for both wavelengths, respectively.

Doubly ionized parent molecules ($CpMn(CO)_3^{2+}$) were not observed in the mass spectra at 805 nm for laser energies lower than 200 μJ. Since the intensities used in the pump–probe experiments are by at least a factor of two lower than the aforementioned one, a further analysis of double ionization

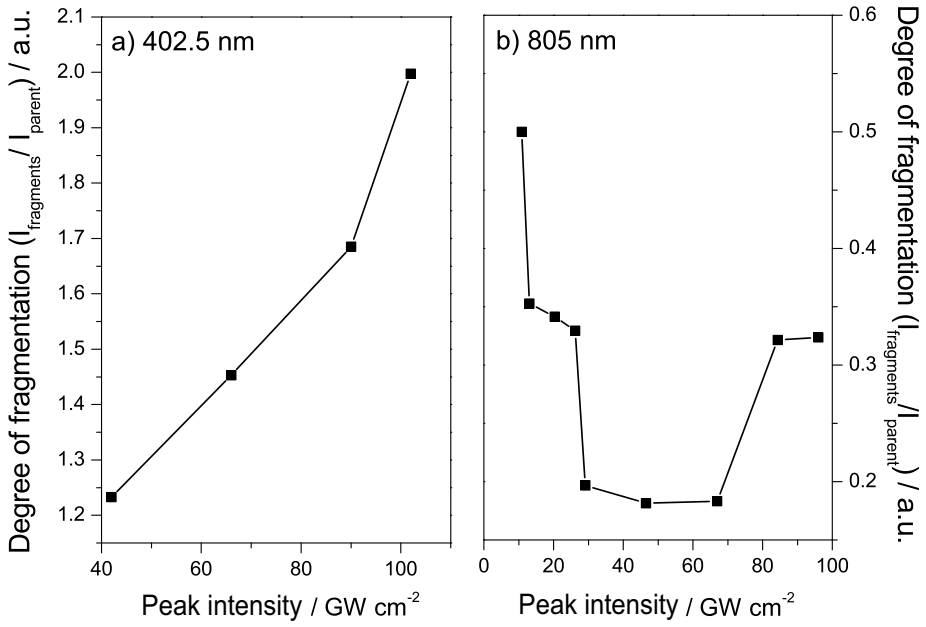

Figure 6.7: The degree of fragmentation ($I_{fragments}$ / I_{parent}) plotted as a function of the laser pulse peak intensity for 402.5 nm (a) and 805 nm (b).

phenomena is not necessary. No multiple ionization was observed in the mass spectra recorded at 402.5 nm for all different laser energies, as well.

Time-resolved Mass Spectra

In order to gain information about the time scale of the fragmentation process, time-resolved mass spectra are measured. This was done by using two laser pulses. The time delay between the pump (402.5 nm) and the probe (805 m) pulse is changed from 80 fs to 210 fs. The peak intensities of the two laser pulses was I_{pump} = 2.36 GW cm^{-2} and I_{probe} = 16 GW cm^{-2}, respectively. The evolution of the ionic product fractions with respect to the delay time between the two pulses was observed (see Figure 6.8). For this reason the obtained mass spectra were normalized to 1 of the $CpMn(CO)_3^+$ ion signal intensity. Progressive increase of all fragment ions fractions with increasing the time delay between the two pulses is clearly resolved as depicted in Figure 6.8. This reveals an ultrafast photo-dissociation of the mother molecule up to the naked Mn^+ on a sub-picosecond time scale. At longer time delays (picoseconds) one would expect a complete wash-out of the parent ion and a pronounced increase of the fragment ions.

The mass spectrometric studies revealed the sensitivity of the system on the employed laser wavelength and pulse energy. This fact can be understood

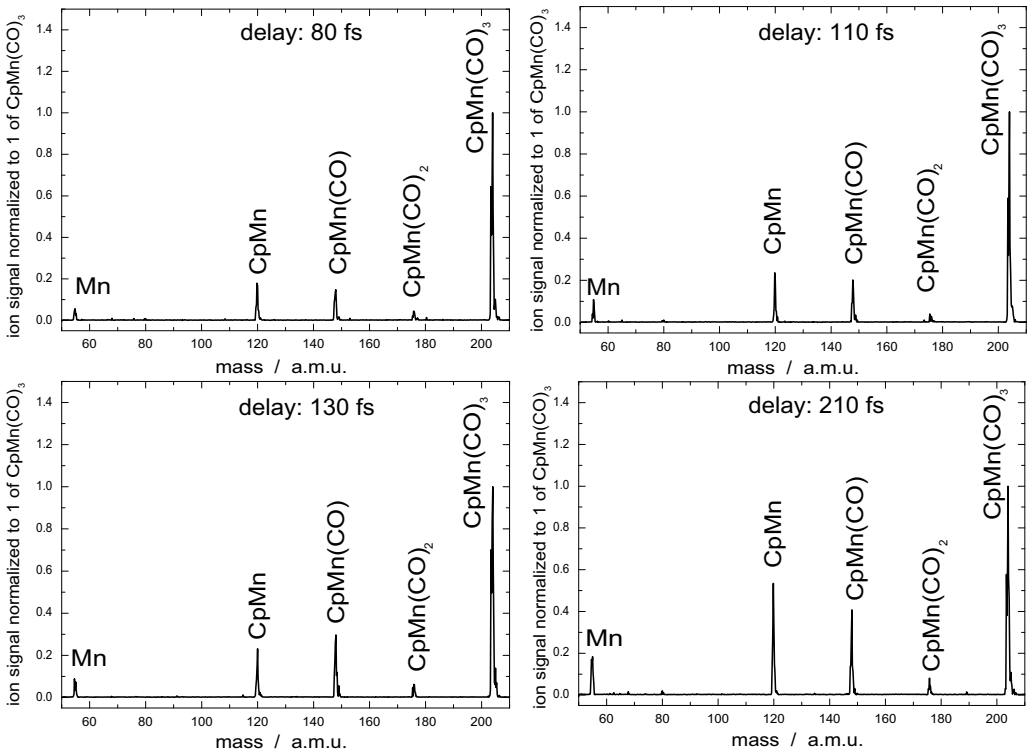

Figure 6.8: Time-resolved mass spectra recorded at different time delays between the pump and probe pulses. λ_{pump} = 402.5 nm; I_{pump} = 2.36 GW cm^{-2}; λ_{probe} = 805 nm; I_{probe} = 16 GW cm^{-2}.

with the model of population of other intermediate states of different species, which contribute to the fragmentation process. However we can not exclude the explanation of fragmentation in ionic states at high laser energies given by Trushin and co-workers [122–124,131,132]. The attempt of the present studies is to investigate if the dynamics observed in the pump–probe experiments, described in the following section, occur on electronic excited states or in ion states.

These results show that the investigation of dynamics occurring on electronic excited states by means of femtosecond pump–probe spectroscopy is more appropriate by employing low laser intensities. At high laser intensities fragmentation would take place after ionization, which would complicate the interpretation of the data. For this reason, only low laser intensities are chosen in the pump–probe experiments. They are described in the next section. A comparison between experiments performed at low and high pump pulse intensities is presented later.

6.3.2 Pump-Probe Spectroscopy on $CpMn(CO)_3^+$ and its Fragment Ions with ca. 100 fs Pulses

In these preliminary experiments, the laser system FS I is used. The duration of the pump and probe pulses was 110 fs and 90 fs, respectively. The excitation pulses of 10 μJ energy are centered at 400 nm and the probe pulses of 30 μJ energy at 800 nm [127]. The polarization of the two laser fields is orthogonal with respect to each other. In order to avoid ionic fragmentation, the laser energies employed in the pump–probe experiments are lower than the energies used in the mass spectrometric studies (see section 6.3.1). In the excitation process, the pump pulse excites the parent molecule in an one-photon transition. The kinetics of the created wave packet is monitored by the probe pulse, which ionizes the excited molecules by a three-photon transition. The laser pulse peak intensity was about 10 GW cm^{-2}.

Figure 6.9 shows the transient spectra recorded at the employed wavelengths for the parent ion $CpMn(CO)_3^+$ and its fragment ions, $CpMn(CO)_2^+$, $CpMn(CO)^+$ and $CpMn^+$. The x-axis represents the time delay between the pump and probe pulses, whereas the y-axis reflects the ion current signal (in arbitrary units). The solid lines are the numerical fits of the measured transients which are obtained after deconvolution. The resulting exponential decay times together with the peak shifts of the transient signal maxima is also displayed in Figure 6.9. Table 6.1 summarizes the peak shifts and decay times obtained after analyzing the corresponding time-resolved spectra for each species. As time zero between the pump and probe pulses the maximum of the $CpMn(CO)_3^+$ transient signal is taken as reference for the time evolution of the measured signals.

The progressive shift of the pump–probe spectra observed in the molecular system indicates the population of different intermediate states involved in the multi-photon fragmentation and ionization processes leading to the formation of individual ions.

The experimental decay time of 66 fs measured for the parent molecule, $CpMn(CO)_3^+$ is in good agreement with the first theoretical calculated value of 63 fs [127]. This time can be interpreted as the cleavage time of the first CO ligand from the metallic core. Furthermore, the theoretical analysis reflects that this first dissociation step occurs on different electronic excited states of $CpMn(CO)_2$ [127].

In the experiments performed by Trushin and co-workers on a number of group-6 metal carbonyl systems, the dissociation process may be a competing process against internal conversion through the conical intersections between two states [122]. Indeed, the fragment $CpMn(CO)_2$ may have enough excess energy to release a second CO ligand. Alternatively, based on purely ener-

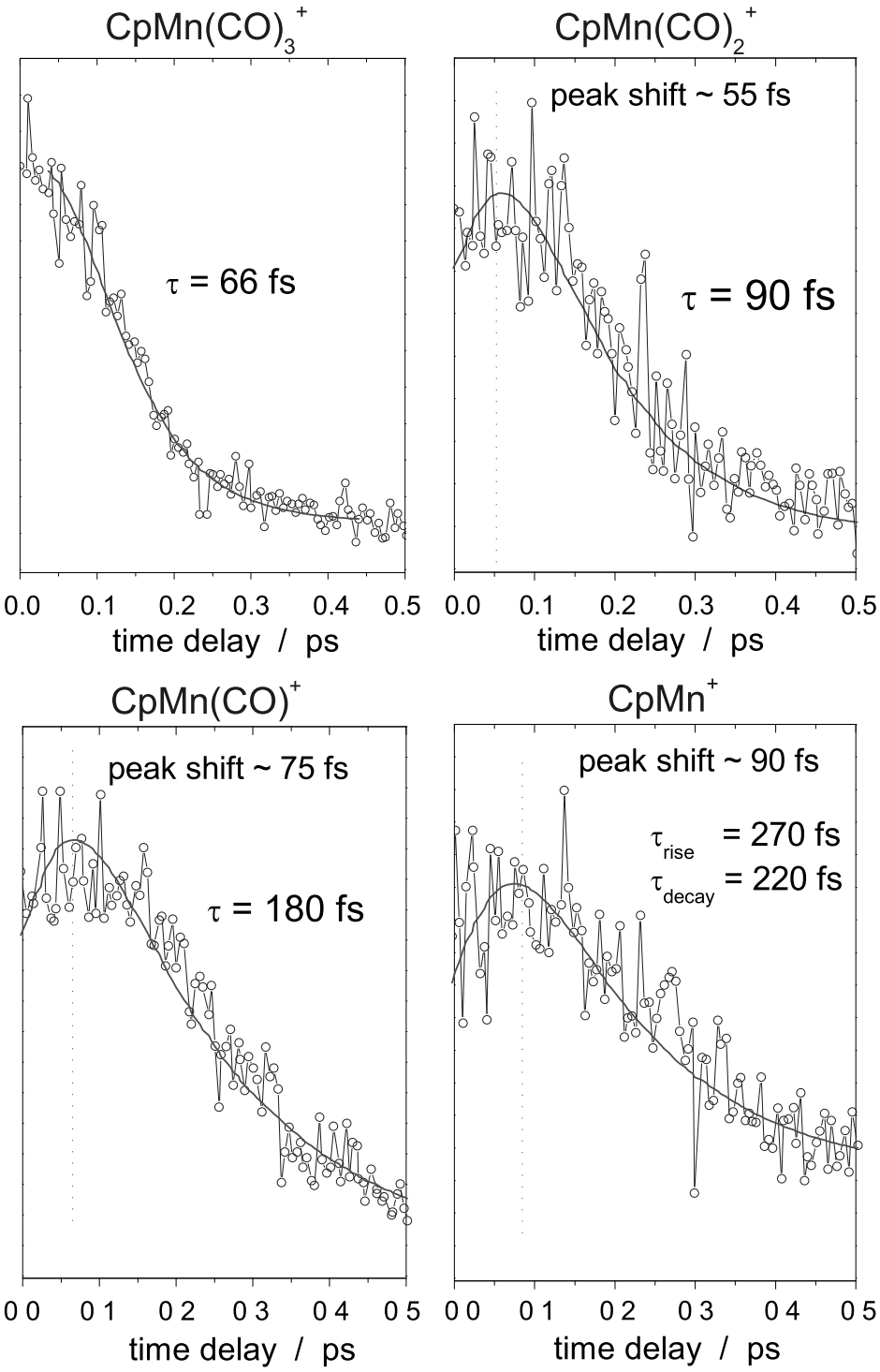

Figure 6.9: Pump–probe traces reflecting the time evolution of the ion signal for $CpMn(CO)_3^+$ as parent molecule and its ion fragments [127]. The corresponding lifetimes of the individual species together with the peak shift of the time-resolved signal is plotted as well.

Measured signal	Peak shift / fs	Decay time / fs
$CpMn(CO)_3^+$	0	66
$CpMn(CO)_2^+$	55	90
$CpMn(CO)^+$	75	180
$CpMn^+$	90	220

Table 6.1: Peak shifts of the transient maxima and the corresponding decay times measured for $CpMn(CO)_3^+$ and each of its fragment ions. λ_{pump} = 400 nm, λ_{probe} = 800 nm. As zero of time delay between the pump and the probe pulses, the maximum of the $CpMn(CO)_3^+$ transient is taken.

getic considerations, the high energy of the pump photon (3.1 eV) would be sufficient to cleave two CO ligands from the parent molecule, $CpMn(CO)_3$.

Thus the exponential decay time measured in the case of $CpMn(CO)_2$ may reflect two processes:

a) the loss of a second CO ligand from the electronic excited $CpMn(CO)_2^*$, or

b) cleavage of the Mn-CO bond from the ground state of this molecule following fast electronic relaxation [127].

The processes mentioned above could be valid in the case of the CpMn(CO) fragment. The two time constants τ_{decay} = 220 fs and τ_{rise} = 270 fs, which describe the decay and the rise time of the $CpMn^+$ transient ion signal, may represent the contribution of different precursors, which can be created via other reaction channels. An intuitive assignment of these time constants can not be made at this point. The mechanism can include population of a variety of intermediate states and a number of channels and ionic fragmentation. One can also consider these multiple pathways which lead to the production of other ion fragments: $CpMn(CO)^+$, $CpMn^+$ and Mn^+ [122] via ionic decomposition [124]. These alternative reaction channels could induce competing ionic fragmentation pathways, which might lead to formation of $CpMn^+$, much faster than CO dissociation from the neutral intermediate CpMn(CO).

No oscillatory behavior of the wave packet was resolved. This might be due to the relatively long time duration of the pump and probe pulses, which hindered the observation of wave packet vibrations in the Franck-Condon ionization window. It appears that in order to reveal any possible wave packet dynamics, shorter pulses are necessary (see next section).

6.3.3 Pump-Probe Spectroscopy on $CpMn(CO)_3^+$ and its Fragment Ions with ca. 40 fs Pulses at Low Pump Pulse Intensities

The goal of this experiment is to resolve the wave packet dynamics in the parent molecule $CpMn(CO)_3$ and its fragment ions by means of ultrashort femtosecond laser pulses.

For these measurements, the FS II laser system was used. The pump and probe pulses have a time duration of 45 fs and 35 fs at FWHM, respectively. The central wavelength is 402.5 nm for the pump pulses and 805 nm for the probe pulses. The employed intensities of the two transform-limited pulses are 2.36 GW cm^{-2} (pump) and 16 GW cm^{-2} (probe), assuming a $sech^2$ pulse. This corresponds to 4 μJ for the pump pulse and 110 μJ for the probe pulse. The polarization of the two laser fields is orthogonal with respect to each other. The photons within the spectrum's envelope would excite other electronic states located around 400 nm (see previous section).

The transient signals of the parent $CpMn(CO)_3^+$ together with its fragment ions, recorded under the aforementioned experimental conditions, are shown in Figure 6.10.

In the case of the parent ion (Figure 6.10a), the transient reflects a modulation of the ion signal with a period of 85±15 fs superimposed on an apparent decay (without deconvolution) of 145 ± 15 fs. The dynamical processes in the cyclopentadienyl ring occur on a time scale of tens of femtoseconds and can be observed with photons in the ultraviolet spectral domain, requiring higher excitation energies. The oscillations, visible up to 200 fs, can be attributed to the Mn–CO bond elongation. Data smoothing through the measured points (the solid line in Figure 6.10a) emphasizes the oscillations. The peak maximum appears at 80 ± 10 fs. The zero-of-time delay $\Delta t_0 = 0$ fs between the pump and the probe pulses was determined by recording the transient signal of the ionized carrier gas.

In the spectrum also for the first fragment ion, $CpMn(CO)_2^+$ an oscillatory pattern with a period of $T_{osc} = 85 \pm 15$ fs is visible (see Figure 6.10b). This oscillation period is equal to the oscillation period of the parent molecule. Thus the parent ion left a fingerprint of its vibrational pattern in the pump–probe trace of the fragment ion. The peak maximum in the transient curve is shifted by 100 ± 15 fs with respect to time zero of delay between the pump and probe pulses. The apparent decay time on which the oscillations are superimposed is 170 ± 15 fs.

The transient spectrum of the $CpMn(CO)^+$ fragment ion is presented in Figure 6.10c. The peak maximum of the $CpMn(CO)^+$ pump–probe spectrum

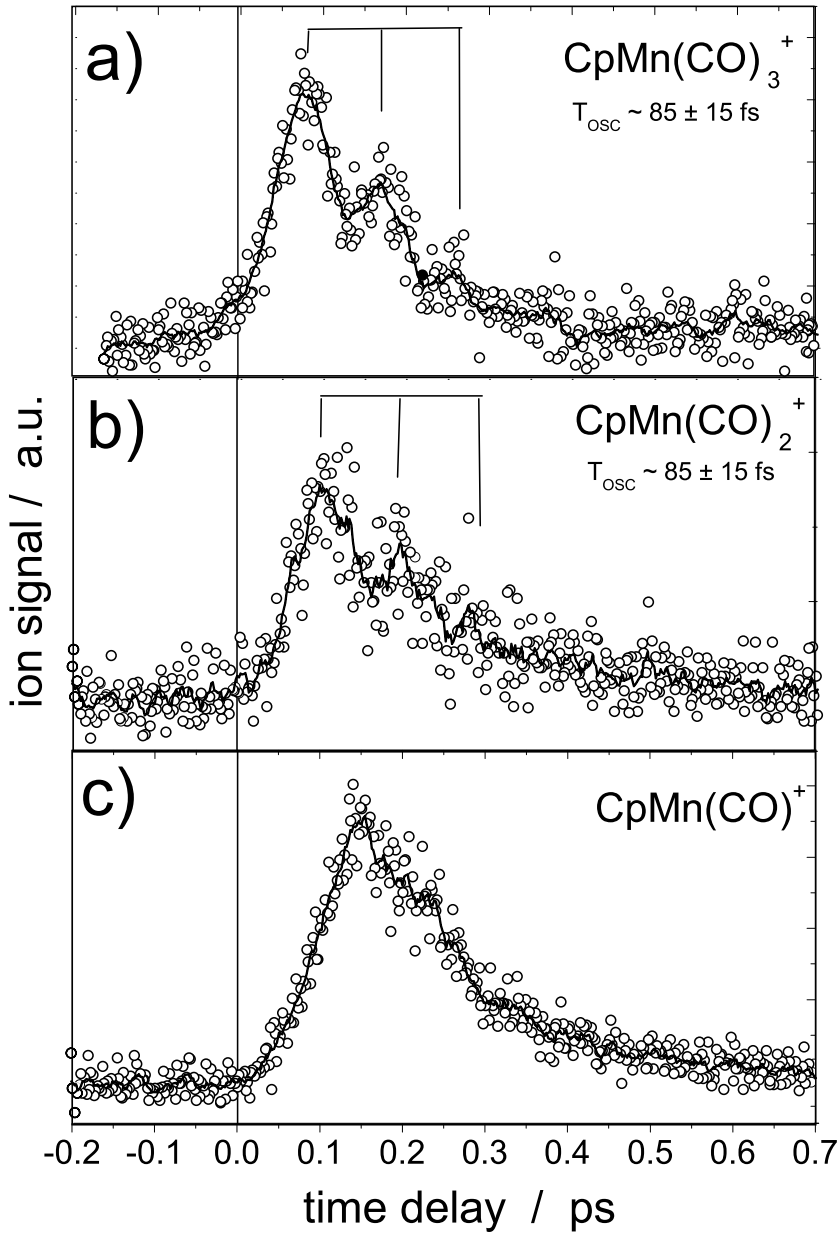

Figure 6.10: Time-resolved spectra on the $CpMn(CO)_3^+$ compound and its fragment ions (dots) recorded with pump pulses of 45 fs centered at 402.5 nm and probe pulses of 35 fs at 805 nm. The ultrafast vibrational dynamics of the parent ion as well as its first fragment ion superimposed on an exponential decay time are clearly resolved up to 200 fs. Each point in the pump–probe trace from Figure 6.10 represents the average value of 10 consecutive measurements. (Dots – the measured data; lines – smoothing using adjacent averaging.

is shifted with approximately 140 fs with respect to the time zero between the pump and the probe pulses. The apparent decay time is about 190 ± 15 fs and reflects probably the decay time of the fragment ion from one or more species which can arise via several reaction pathways. No assignment can be made for this decay time, but one should take into account that there are a variety of reaction channels. Moreover, no dominant oscillations of the ion signal were observed for this species.

The analysis of the real-time spectra (oscillations and the decay pattern) for the parent $CpMn(CO)_3^+$ and its first fragment $CpMn(CO)_2^+$ is of an undoubted importance for decoding the mechanism hidden in the optimal pulse, described in the next section. In order to explain the measured pump–probe signals from Figure 6.10, an accurate theoretical analysis is necessary.

In the group of Manz *ab initio* treatment of potential energy curves and adiabatic couplings of the neutral and ionic parent molecule $CpMn(CO)_3$ was performed [121, 127, 133]. The dynamics is monitored along the one-dimensional dissociative Mn–CO reaction coordinate. The calculated pump–probe spectrum together with the experimental results for $CpMn(CO)_3^+$ and its fragment ion $CpMn(CO)_2^+$ are depicted in Figure 6.11a and Figure 6.11b, respectively. The x-axis represents the time delay between the pump and probe pulses (in both theory and experiment), whereas on the y-axis the measured ion signal (left) and the calculated ion population (right) are indicated. The experimental and calculated pump–probe traces are in excellent agreement [133].

The pump–probe traces can be explained on the basis of the potential energy diagram containing the involved surfaces shown in Figure 6.12. The potential curves which participate in the wave packet dynamics are the electronic ground state (noted X), three electronic excited states (noted a, b, c) and two ionic states (noted a^+, b^+)[1].

The analysis of the theoretical wave packet dynamics helps understanding the mechanism of the pump–probe experiments. The pump pulse prepares a wave packet from the ground state X to three excited states: a, b and c. The wave packet generated in the c-state does not contribute to the transient signal, since the frequency of the probe pulse is off-resonant. From the predissociative b state, the wave packet decays to the a state within and apparent decay time of $\tau_{theory} = 166$ fs. This decay time was theoretically calculated by fitting an exponential to the time-dependent population of the b state [121,133]. The theoretical decay time agrees well with the experimental decay time of $\tau_{exp} \sim 145 \pm 15$ fs obtained from the measured transient.

[1]For simplicity, the electronic states notation is abbreviated. In Ref. [133] X stands for a^1A', a for a^1A'', b for b^1A'', c for c^1A', a^+ for $(a^2A'')^+$ and b^+ for $(b^2A')^+$.

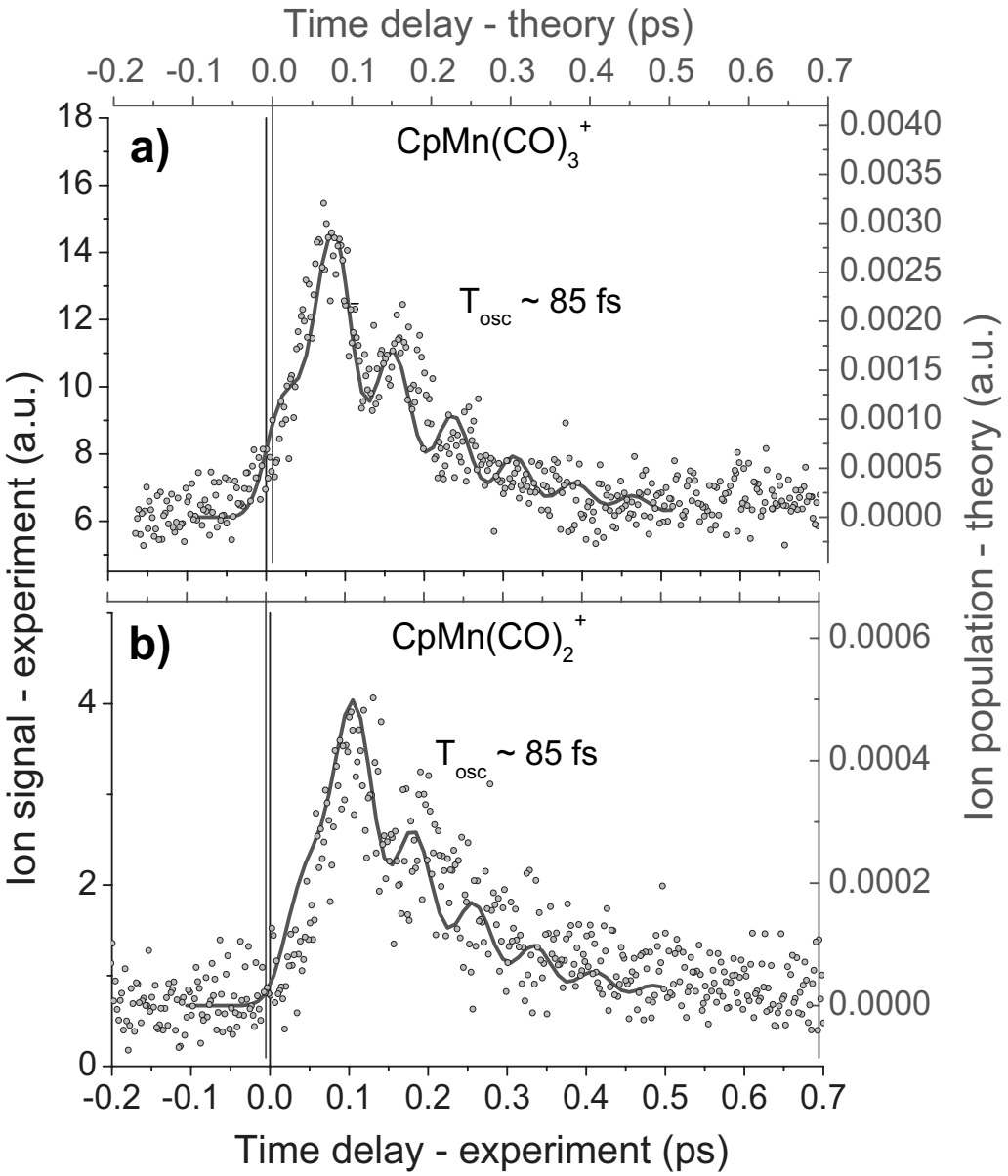

Figure 6.11: Experimental (dots) and theoretical (solid line) femtosecond pump-probe spectra of $CpMn(CO)_3^+$ (A) and its fragment ion $CpMn(CO)_2^+$ (B). The small differences in the peak shifts of 10-15 fs between the theoretical and experimental spectra are due to the errors present in the experiment and theoretical calculations [133].

Simultaneously, the wave packet vibrates also in the b state with a period of $T_{osc} = 85 \pm 15$ fs, but every time it passes the point of vicinity between b and a states (near 1.78 Å), a portion of the wave packet leaks out into the dissociative a state. The formed fragment ion, $CpMn(CO)_2^+$, can be probed with the same probe wavelength of 805 nm to the a^+ ionic state. Thus in the case of the parent ion $CpMn(CO)_3^+$ there are two competing processes: ionization and fragmentation into $CpMn(CO)_2^+$. These features were successfully exploited in the optimal control experiments from Ref. [133].

The wave packet dynamics (initial preparation and periodic decay) is monitored by the probe pulse, which ionizes the parent molecule into the ionic b^+ state. The first peak in the pump–probe spectrum appears after $\Delta t = 80 \pm 15$ fs. This time is required by the wave packet to arrive at the Franck-Condon window of ionization and is the result of three competing effects:

i) the time the pump pulse requires to populate the b excited state,

ii) the time in which the wave packet propagates towards the outer turning point during its first vibration on the b state,

iii) the decay time in which the wave packet leaks into the ultrafast dissociative a state.

After decaying on the a excited state fragment ions are formed, which can be probed at the same frequency to the a^+ ionic state. The probe pulse transfers also a small fraction of the dissociative state a to the ionic ground state of the daughter ion, namely a^+.

The contribution of the wave packet in the c excited state to the two-color transient spectrum is negligible because of the off-resonant probe frequency, although the dynamics in this state is very important for deducing the control mechanism, as it will be shown in the next section. According to the theoretical calculations [133], the vibrational dynamics in the c state have a period of 170 fs, and the decaying pattern is negligible.

Figure 6.11b presents the pump–probe trace of the first fragment ion $CpMn(CO)_2^+$. An oscillation pattern with the period of $T_{osc} = 85 \pm 15$ fs is visible. The vibrational period is equal with the one observed for the parent ion (see Figure 6.11a). The first maximum appears after roughly 100 fs with respect to the overlapping time of the pump and probe pulses $\Delta t_0 = 0$ fs. The approximately 20 fs time delay with respect to the peak maximum observed in the $CpMn(CO)_3^+$ transient spectrum corresponds to the time required by the wave packet in the a state to travel from its origin (the near-coincidence point between b and a states) to the probe window. Apparently this additional time is needed by the wave packet to proceed on the predissociative a state to a Franck-Condon window for ionization. This time delay is a consequence of a new born species. The oscillations in the $CpMn(CO)_2^+$ transient, reflecting

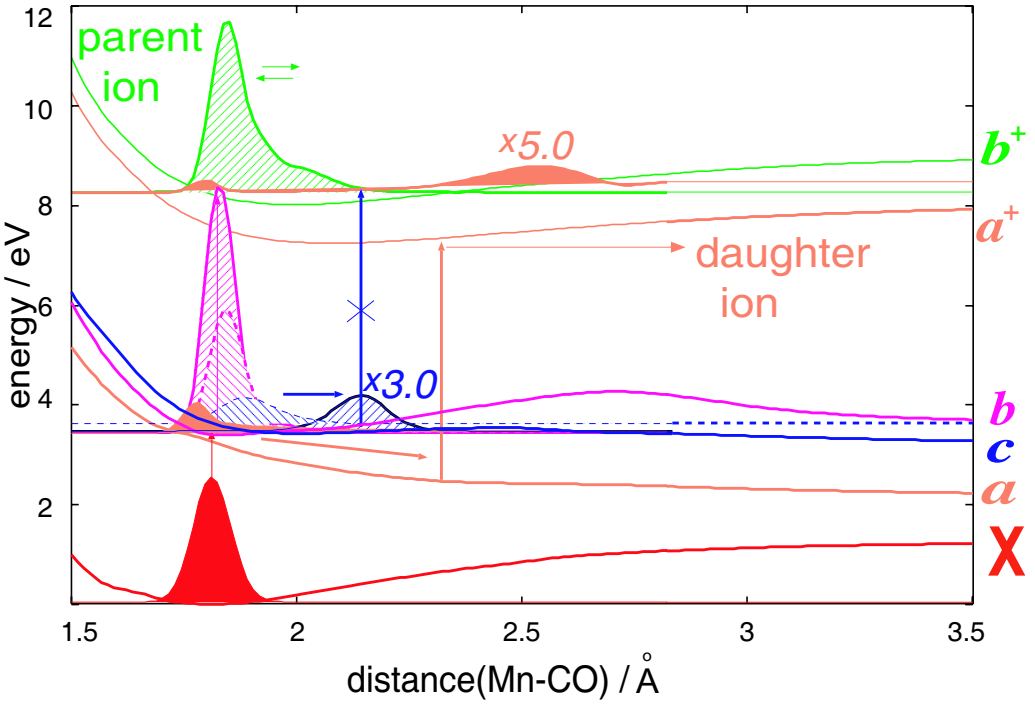

Figure 6.12: Potential energy curves calculated for $CpMn(CO)_3$ [133]. The involved electronic states are the following: X is the electronic ground state; *a*, *b* and *c* are the electronic excited states involved and a^+, b^+ the ionic states.

the elongation of the Mn–CO bond, are superimposed on an apparent decay time of 170 ± 15 fs.

The two-color time-resolved analysis on the other fragment, $CpMn(CO)^+$ is displayed in Figure 6.10c. No dominant oscillations were resolved for this species. The apparent decay time is 190 ± 15 fs. The maximum of the $CpMn(CO)^+$ pump–probe trace is shifted by 140 fs, due to the delayed cleavage of the Mn–CO bond. The elimination of CO ligands might take place on intermediate excited state(s) of different species, which are populated in the multi-photon process. The $CpMn(CO)^+$ transient reflects probably the rise and decay time of the fragment ion from the two precursors which can arise via different reaction pathways. The $CpMn(CO)^+$ formation could also occur via competing fragmentation paths in the ionic state, which is faster than via the intermediate excited states of the neutral $CpMn(CO)_2$.

Since the first maximum is most pronounced for all transients, we are able to conclude that the ionization is very efficient during the first passage of the wave packet through the Franck-Condon ionization window. This phe-

nomenon has been previously reported in Ref. [122]. (Therein it was stated that the ionization probability depends on the position of the wave packet on the potential energy surfaces.)

6.3.4 Interpretation of the Optimal Pulse for $CpMn(CO)_3^+$ Ionization

The experimental and theoretical efforts on the analysis of the pump-probe spectra allowed a closer investigation of the mechanism of the optimal laser pulse obtained for the optimization of $CpMn(CO)_3^+$ ion yield.

Previous adaptive control experiments on $CpMn(CO)_3^+$ are described in Ref. [59]. Therein it was shown that a single non-optimized transform-limited pulse of 10 nm (at FWHM) centered around 800 nm produces both parent and fragment ions. The task of the optimization algorithm was to maximize the photo-ionization process of $CpMn(CO)_3^+$ and to hinder any loss of ligands. This is illustrated in Figure 6.13: the subject of optimization was the parent ionization (channel (1)), while fragmentation in $CpMn(CO)_2^+$ is suppressed (channel (2)). In order to operate in a roughly linear regime, only the phase of the laser pulse was modulated. This is because amplitude modulation would change the pulse energy during the iterative optimization.

The optimal pulse obtained after performing the adaptive feedback control experiment on $CpMn(CO)_3^+$ ionization and after the corresponding phase-retrieval analysis is depicted in Figure 6.14. During the optimization experiment, a monotonic progression of the parent ion signal is observed (see the inset in Figure 6.14). In the beginning, the evolutionary algorithm starts with random phase values (free optimization). This corresponds to pulses spread over several picoseconds, which leads to a low ion signal (region (a)). The progression of the ion signal overcomes the ion signal produced by a short pulse (region (b)) and reaches convergence after approximately 90 generations (region (c)). The optimization factor, representing the ratio between the intensity of the ion signal produced by the optimal pulse and the intensity of the ion signal generated by the short pulse amounts $I_{opt}/I_{short} = 1.6$. The relative ratio of the parent ion $CpMnCO_3^+$ to the first fragment ion $CpMnCO_2^+$ after the optimization, obtained from the mass spectra recorded with the optimal pulse [59] is even larger (2.06).

The optimal pulse for the $CpMnCO_3^+$ was measured with the SHG-FROG and its intensity and phase profile were retrieved with the FROGGUI software by means of the generalized projections algorithm. A description of the shareware programm is given in Appendix B. The intensity distribution of the optimal pulse, depicted in Figure 6.14, reveals three intensity

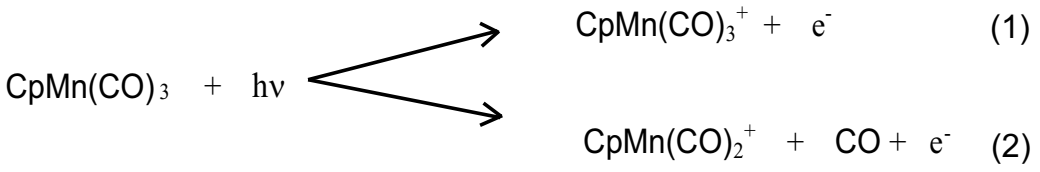

Figure 6.13: The two competing possible pathways: formation of the parent ion ($CpMn(CO)_3^+$) vs. loss of one CO ligand and formation of the daughter ion ($CpMn(CO)_2^+$).

maxima (subpulses): the two dominant pulses are separated in time by $\Delta t_{1,2} = 85 \pm 15$ fs are followed by a third, less intense, maximum situated after $\Delta t_{2,3} = 85 \pm 15$ fs. The time duration of the subpulses is about $\Delta t = 40$ fs at FWHM.

After a quantitative analysis of the optimal phase (polynomial fit), the wavelength shift of each subpulse could by assigned. The first subpulse contains higher frequency components of the input pulse (798.7 nm). The blue shift of $\hbar\Delta\omega = 0.0026$ eV (1.3 nm) is in a good agreement with the theoretical calculated value of 0.0024 eV [121]. The second subpulse is slightly shifted with 0.09 nm towards redder wavelengths (800.09 nm) and the third subpulse is also red-shifted to 801.12 nm compared to the central wavelength of the transform-limited pulse.

The temporal profile of the optimal pulse would intuitively suggest an excitation of the parent molecule on an electronic excited state (resonant to 400 nm). From here, after approximately 85 fs time delay the molecular configuration is favorable for a transition to an ionic state performed by the second subpulse. The third subpulse suggests a second ionization step of a residual wave packet which is generated by the second subpulse on the same electronic excited state, and ionized after approximately 85 fs. This hypothesis will be verified in this section.

Pump–probe spectroscopy and theoretical calculations with pulses as short as the ones of the optimal pulse (ca. 40 fs), described in the previous section, help deciphering the control mechanism "hidden" in the optimal pulse.

The task of the optimization procedure is to increase the photo-ionization process of $CpMn(CO)_3^+$. Thus the evolutionary algorithm should avoid preparing a wave packet in the b state. This would transfer the population into the repulsive a state, which would lead to the undesired formation of the fragment ion, $CpMn(CO)_2^+$.

In order to increase the ion signal as much as possible, the optimization method has to excite the molecule preferably in the c state, which is located slightly above the b state (see Figure 6.15). This is consistent with the central

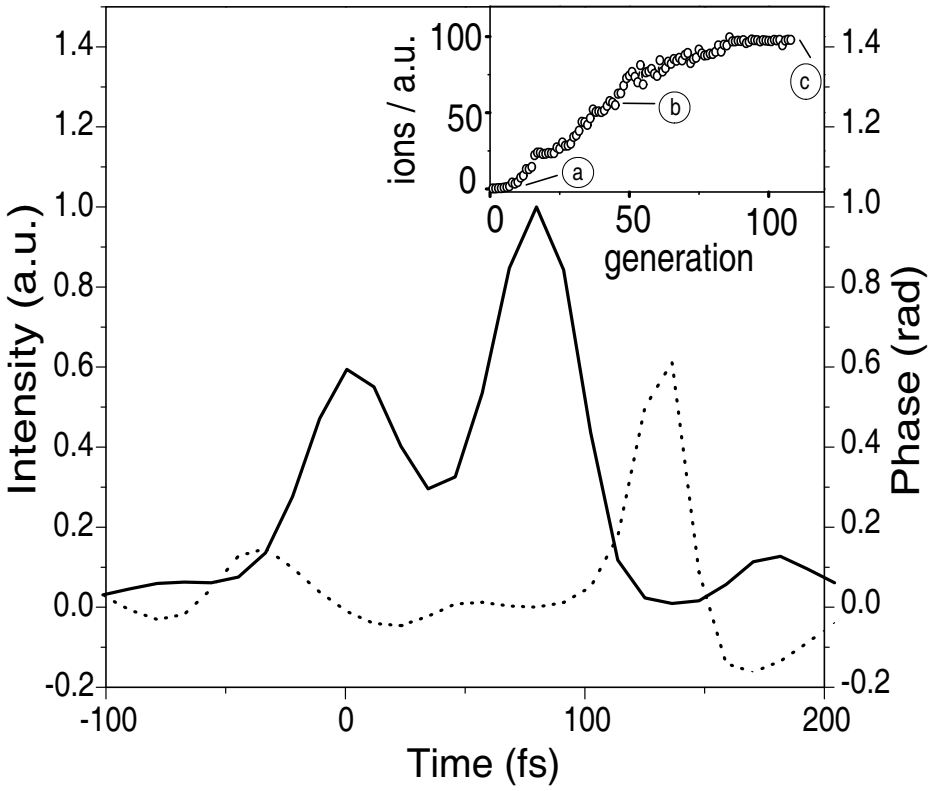

Figure 6.14: The intensity (solid curve) and the phase profile (dotted curve) of the optimal pulse obtained for maximization of the $CpMn(CO)_3^+$ ion yield. The temporal separation between the subpulses is 85 ± 15 fs. The inset represents the evolution of the ion signal during the optimization procedure as a function of iteration number.

wavelength of the reference unshaped pulse (800 nm), which is shorter than the wavelength used in the pump–probe experiments ($2 \times 402.5 = 805$ nm).

Thus the first subpulse creates a wave packet in the c state, which lies above the b state [133]. The choice of the cental wavelength of the reference pulse (800 nm), which is slightly shorter than the wavelength used in the pump–probe experiments ($2 \times 402.5 = 805$ nm) allows this transition. The shift of 1.3 nm to higher frequency components (798.7 nm) with respect to the input laser field (800 nm) within the first subpulse might be responsible for a successful excitation. The wave packet starts to propagate along the potential well of the c state. After approximately 85 fs, corresponding to half period in the c state, the wave packet is located at the outer turning point. At this position the Franck-Condon factors are favorable for a vertical transition from the c state to the ionic state b^+.

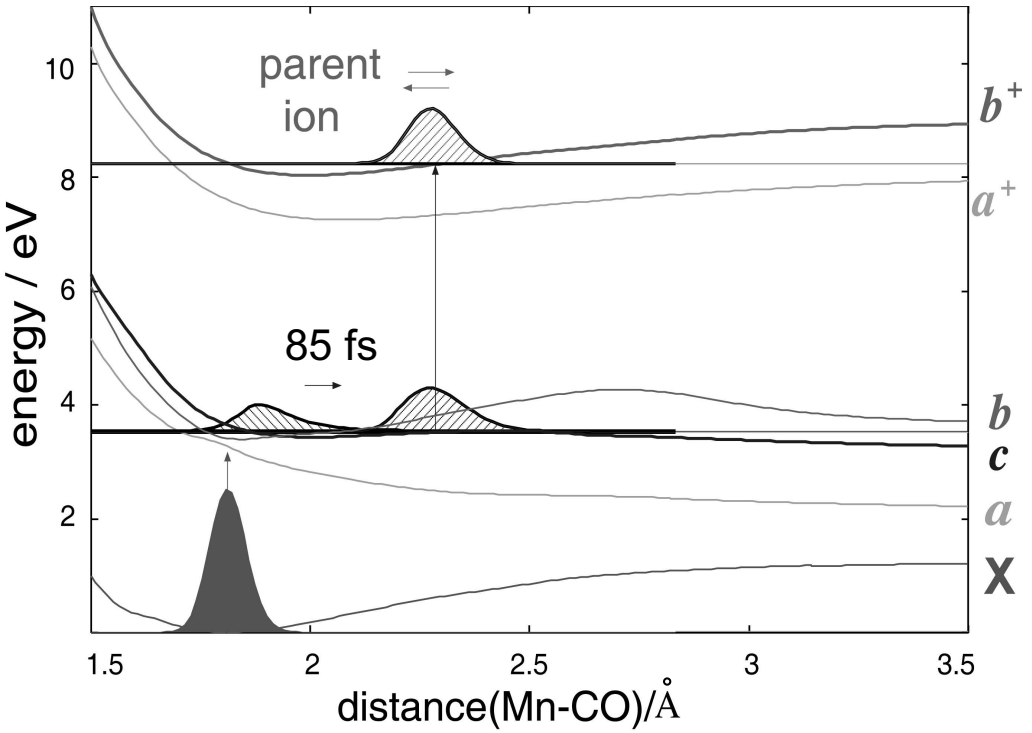

Figure 6.15: The potential energy curves calculated for $CpMn(CO)_3$ involved in the control experiment: the electronic ground state X, the electronic excited state *c* and the ionic state b^+. The optimal pulse avoids the wave packet generation in the *a* state [133].

The feedback loop produces a second subpulse in order to perform the $b^+ \leftarrow c$ transition (see Figure 6.14). Thereafter the ionization step is optimized as well, without an excursion of the wave packet on the dissociative state *a*. The red-shift is, however, not large enough to induce efficient transition to the *b* state and the phase of the second subpulse can be considered constant. The second subpulse could generate an additional population in the *c* state, which is ionized by the third sub-pulse. This "residual" population is later ionized by the third, least intense, subpulse of 801.12 nm central wavelength after another time delay of 85 ± 15 fs.

It is worth mentioning that in the optimization experiment the relative phase of the optimal pulse is designed by the learning loop in order to prepare appropriate spectral components at the right time. In this way, a successful excitation at the inner turning point of the *c* state and ionization of the parent molecule from the outer turning point of the *c* state is achieved by the chirped subpulse(s).

The process of decoding the control mechanism performed by the opti-

mal pulse was possible by using femtosecond high-resolution pump–probe experiments and theoretical *ab initio* quantum calculations and wave packet dynamics simulations [133].

6.3.5 Pump-Probe Spectroscopy on $CpMn(CO)_3^+$ and its Fragment Ions with ca. 40 fs Pulses at Higher Pump Pulse Intensities

This experiment tried to inquire if by increasing the peak intensity of the pump pulse the ultrafast fragmentation processes in $CpMn(CO)_3^+$ and its fragment ions still occur in electronic excited states or the wave packet is transferred in dissociative ion states. In the experiment presented in section 6.3.3, the peak intensity of the pump pulse was approximately 2.4 GW cm^{-2}.

In the experiment described in this section, the pulse duration remain constant, i.e. 45 fs for the pump pulse and 35 fs for the probe pulse. The peak intensity of the pump pulse is now increased to 9.6 GW cm^{-2}, whereby the probe pulse intensity stays almost the same (17.5 GW cm^{-2}). This corresponds to a pulse energy of 16 μJ for the pump pulse. The probe pulse energy is 125 μJ. The central wavelengths of the pump and probe pulses are 402.5 nm and 805 nm, respectively. The polarization of the two laser fields is orthogonal with respect to each other.

The resulting pump–probe spectra changed significantly in comparison with the traces presented in Figure 6.10. Figure 6.16 displays the transients of the parent ion $CpMn(CO)_3^+$ and its fragment ions recorded with the aforementioned laser intensities.

All the spectra are dominated by an increase of the ion signal with a maximum around 90–110 fs with respect to time-zero of delay followed by an exponential decay. The fact that the peak maxima of all measured kinetic traces appear at almost the same time suggests that this could be a consequence of an simultaneous loss of ligands of the parent $CpMn(CO)_3$ [130]. The decay times for the investigated species were determined to be 40 ± 15 fs for $CpMn(CO)_3^+$, 100 ± 15 fs for $CpMn(CO)_2^+$ and 100 ± 15 fs for $CpMn(CO)^+$ [130], respectively. A summary is given in Table 6.2. Moreover, no significant oscillatory behavior is observed for any of the investigated molecules. The exponential lifetime of the parent $CpMn(CO)_3$ is much shorter than the apparent decay time observed in Figure 6.10a. This could give hints on the fact that the observed time evolution takes place in another state, other than the excited states a and b (see Figure 6.12).

Due to its higher peak intensity (factor of 4), the pump pulse can transfer

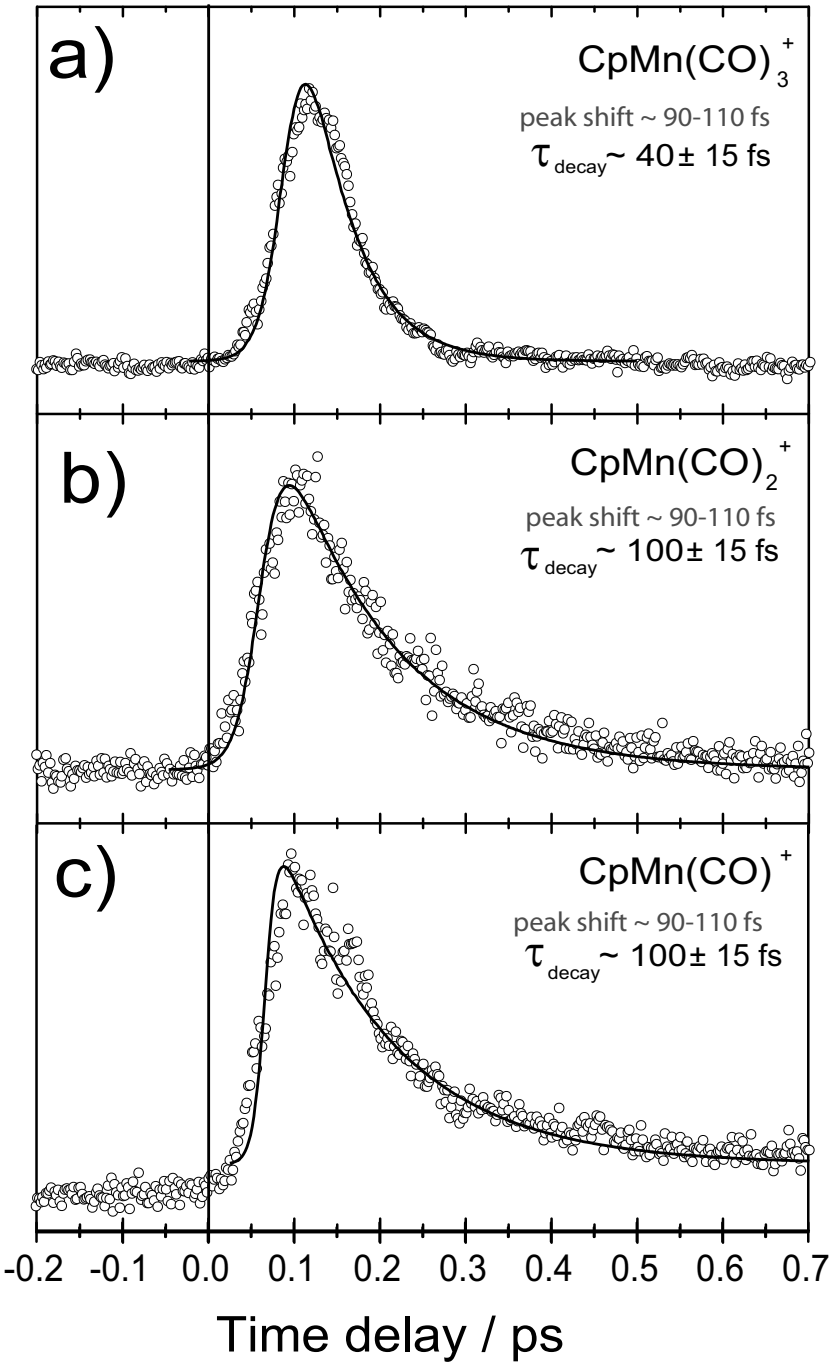

Figure 6.16: Pump–probe trace of $CpMn(CO)_3^+$ (a) and its fragment ions $CpMn(CO)_2^+$ (b) and $CpMn(CO)^+$ (c) recorded at 9.6 GW cm^{-2} pump-photon intensity [130]. No vibrational behavior is visible for both parent ion and its first fragment ion. The employed wavelengths were 402.5 nm (pump) and 805 nm (probe).

Measured signal	Peak shift / fs	Decay time / fs
$CpMn(CO)_3^+$	100–110	40±15
$CpMn(CO)_2^+$	90–110	100±15
$CpMn(CO)^+$	100	100±15

Table 6.2: Peak shifts of the transient maxima and the corresponding decay times measured for $CpMn(CO)_3^+$ and each of its fragment ions with $\lambda_{pump} = 402.5$ nm and $\lambda_{probe} = 805$ nm. The peak intensity of the pump pulse is increased to $I_{pump} = 9.6$ GW cm^{-2}.

the population from the ground state of the neutral parent molecule directly to other state(s). The fragmentation of the parent molecule (Figure 6.16a) can occur in the ionic state, giving rise to the ion fragment $CpMn(CO)_2^+$. Moreover, the probe pulse can also transfer higher kinetic energy to the outgoing wave packet, resulting in $CpMn(CO)_2^+$ ion fragmentation into $CpMn(CO)^+$. The formation of the ionic fragment $CpMn(CO)^+$ can also take place via parent dissociation in the ion, according to Ref. [122].

The fragmentation of the parent molecule $CpMn(CO)_3$ could also occur on the ultrafast predissociative *a* state, because the energy of the pump photon does not change. Nevertheless, the first fragment $CpMn(CO)_2^+$ could appear if the wave packet reaches the ionic state (after being transferred from the repulsive state *a*) and has still enough kinetic energy to overcome the dissociation barrier in the ionic state [121]. The probe photon energy amounts 3 × 1.53 eV; hence, the molecule has sufficient kinetic energy to climb the barrier in the ionic state and to lose one or more CO ligands [130].

6.4 Control of $CpMn(CO)_2^+$ Ionization Process

As described in section 6.3.4 it was demonstrated that for the parent ion, $CpMn(CO)_3^+$, the information coded in the optimal pulse obtained can be extracted by high-resolution femtosecond pump–probe experiments together with *ab initio* theoretical wave packet simulations. Before the optimization the ratio first fragment/parent ion produced by an unshaped pulse was $CpMn(CO)_2^+$: $CpMn(CO)_3^+$ = 1.52:100. After the optimization the ion yield of $CpMn(CO)_3^+$ increased by a factor of 1.6 (see Figure 6.14), whereas the relative ratio $CpMn(CO)_2^+$: $CpMn(CO)_3^+$ was modified to 0.73:100, i.e. by a factor of 0.48 with respect to the ratio produced by a short pulse.

The optimization of the $CpMn(CO)_2^+$ ion yield would give additional information into the ultrafast dynamics involved during the control process. Based on the potential energy curves shown in Figure 6.15 one can expect an optimal laser field consisting of two main subpulses [120]. The first subpulse would excite the mother molecule into the repulsive electronic excited state *a*. Here the molecule dissociates by losing one CO ligand. The second subpulse would arrive after an optimal time delay. Containing the appropriate frequency it would ionize the fragment species. Intuitively, an almost unchirped pulse (or with a small chirp) would be necessary for the excitation of the parent molecule and a strong downchirped pulse would be needed to ionize the fragments after an optimal time delay (see Figure 6.15). The optimal laser pulse expected in the experiment should offer additional information about the mechanism of the optimized process.

6.4.1 Free Phase Optimization of $CpMn(CO)_2^+$ Ion Yield

In the experiment the laser system FS II is used. The input amplified pulses are centered around 805 nm and have a duration of about 180 fs (at FWHM), i.e. 2.8 times longer than a transform-limited pulse assuming a Gaussian shape.

The spatial liquid-crystal modulator (SLM) is placed in the Fourier plane of a zero-dispersion compressor, which is a folded setup of two gratings (600 lines/mm) and two cylindrical-concave mirrors ($f = 130$ mm) in a $4f$-arrangement (see Figure 3.5). In order to avoid the damage of the SLM, in the optimization experiment only 230 μJ were allowed to pass through the liquid crystal mask.

In this experiment only the phase of the input femtosecond pulse is exclusively optimized in order to keep the pulse energy constant. All the 128 parameters $\varphi_n(\omega)$ of the spectral phase are iteratively optimized. This corresponds to the most general optimization case (free optimization).

It is possible that the optimized pulse shapes can slightly differ, while the optimized ion yield is almost the same for a repeated number of optimization experiments. This may be due to high complexity of the parameter space (searching for solutions in a 128-dimensional space), in which the evolutionary algorithm tries to find the best solution. This solution can be reached under our experimental conditions by somewhat different pulse structures, since their deviations in fitness are too small to be distinguished in the selection step. The pulse form presented in this section was frequently obtained in the optimization runs under the given experimental conditions.

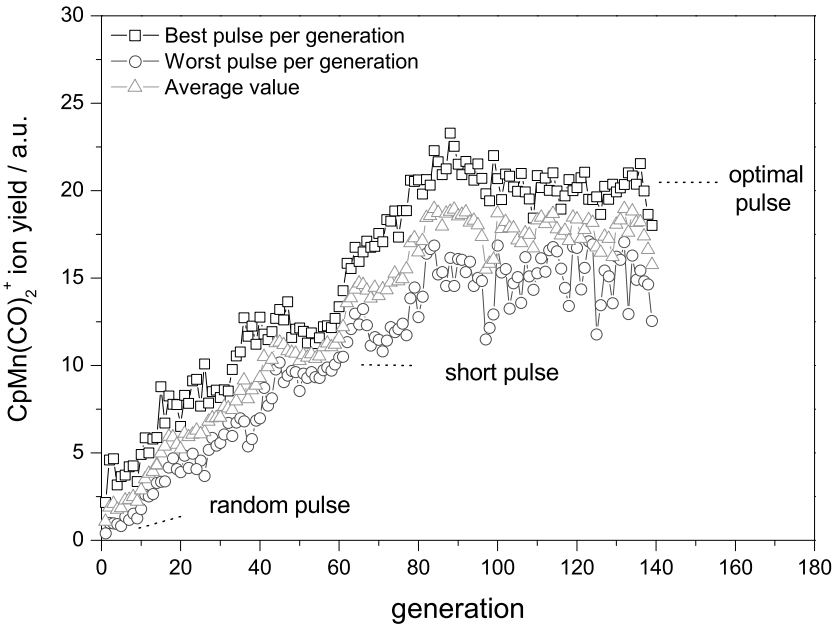

Figure 6.17: Typical progression of the ion yield during the free phase optimization of the $CpMn(CO)_2^+$ at 805 nm.

In Figure 6.17 the learning curve of the optimization algorithm is shown. This is obtained by recording the $CpMn(CO)_2^+$ ion yield for each generation. Although instabilities are present in the molecular beam, the evolutionary algorithm converges after approximately 250 generations. The best individual in one generation might produce a lower ion signal in the next generation if additionally all other individuals generate less ion yield than the previous best one, during molecular beam instabilities. This could lead to a decrease of the ion signal in the evolution of the best individual.

The $CpMn(CO)_2^+/CpMn(CO)_3^+$ mass peak ratio before the $CpMn(CO)_2^+$ ion yield optimization is 1.52:100. After the optimization, the ratio of fragment/parent ion yield is improved by a factor of 1.5 (to 2.3:100) with respect to the ion signal produced by an unshaped pulse. This indicates that the control experiment lead to a substantial increase of the desired product.

6.4.2 Analysis of the Optimal Pulse Form

The time-wavelength profile and the pulse form of optimal laser pulse acquired for $CpMn(CO)_2^+$ are measured by the SHG–FROG technique and shown in Figure 6.18. The FROG trace (Figure 6.18a) exhibits five intensity maxima (subpulses). After the phase-retrieval procedure (FROGGUI, [6]), which gives

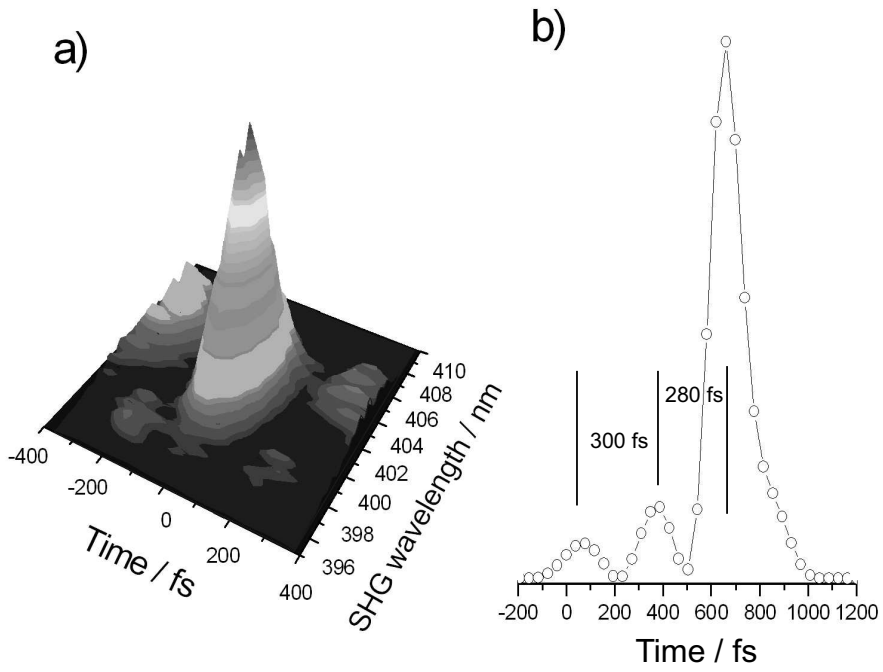

Figure 6.18: The optimal pulse obtained for the process $CpMn(CO)_2 \rightarrow CpMn(CO)_2^+$: (a) The time-wavelength profile of the optimal laser field measured by the SHG FROG technique shows a dominant peak with two wings each left and right, symmetrically distributed around the main pulse; (b) The retrieved intensity of the optimal pulse form displays a pulse sequence which consists of three intensity maxima with time separations of $\Delta t_{1,2} = 300$ fs and $\Delta t_{2,3} = 280$ fs, respectively [134].

the amplitude and the phase of the electric field of the optimal pulse, the corresponding retrieved amplitude consists of three subpulses with the ratios of approximately 1:2:15 (Figure 6.18b).

The time separation between the first two subpulses is approximately 300 ± 15 fs and between the second and the third subpulse is about 280 ± 15 fs. The time duration of the subpulses measured at FWHM is 140 fs, 125 fs and approximately 125 fs, respectively.

Intuitively the time-profile of the optimized pulse might suggest an excitation step performed by the first subpulse. The second subpulse is created approximately 300 fs later. It might ionize the $CpMn(CO)_2^*$ fragment. Since its intensity is twice as high as the first subpulse, it could again excite the

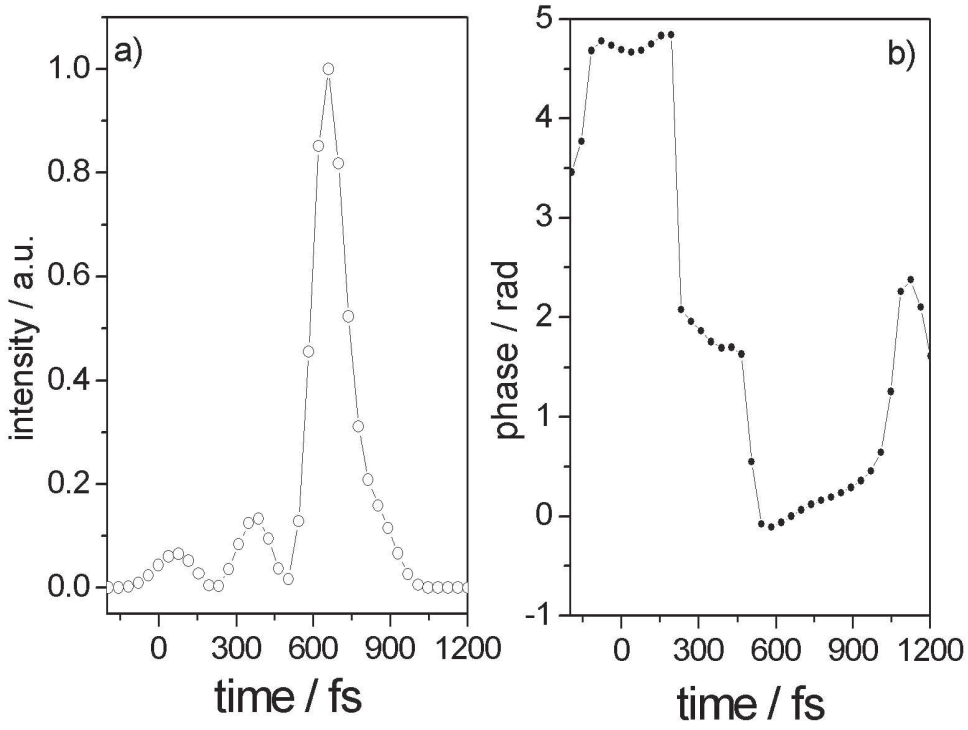

Figure 6.19: The optimal pulse obtained for the process $CpMn(CO)_2 \rightarrow CpMn(CO)_2^+$ after the phase retrieval analysis: (a) The retrieved intensity which consists of three subpulses separated by $\Delta t_{1,2} = 300$ fs and $\Delta t_{2,3} = 280$ fs, respectively; (b) The retrieved phase of the optimal pulse [134].

$CpMn(CO)_3$ molecule from the electronic ground state in one or more of the electronic excited states. After 280 fs, when the third and most intense subpulse arrives, the excited fragment species could be subsequently ionized in a multi-photon step. Simultaneously, the last subpulse could again excite the parent molecule and subsequently ionize its $CpMn(CO)_2^*$ fragments [134].

The corresponding temporal phase of the optimal pulse is reconstructed with the FROGGUI software (see Appendix B). One can distinguish a small downchirp (due to the quadratic phase function) of the first subpulse. In the case of the central and the third subpulse the phase is linear. After a quantitative analysis of the retrieved phase, the central wavelength of the first subpulse is shifted to 805.7 nm with respect to the central wavelength of the input unshaped pulse of 805 nm. An assignment of this wavelength shift can not be made at this point. The linear shift of the spectral phase

observed for the second and third subpulse corresponds to a temporal shift of the pulse in the time domain (see section 3.1.2).

The time separation between the three intensity maxima subpulses is not half of the oscillation period of any of the b or c states (see Figure 6.15). The long time delay between the two subpulses (300 fs and 280 fs, respectively) might be due to repeated oscillations on the involved electronic states and delayed fragmentation into the a state, followed by a multi-photon ionization. This assumptions should certainly be verified in future by theoretical calculations combined with one-color pump–probe experiments.

6.5 Summary and Outlook

This chapter described femtosecond analysis and control experiments on the organometallic molecule $CpMn(CO)_3$.

The mass spectrometric studies performed at 402.5 nm and 805 nm showed the sensitivity of the system on the employed laser pulse energy and central wavelength. A closer investigation of the fragmentation degree gave hints about dissociation occurring on electronic excited states.

The two-color pump–probe experiments allowed the determination of the excited state fragmentation times of the parent molecule and its fragment ions. By employing laser pulses of approximately 40 fs time duration, oscillatory patterns of 85 ± 15 fs time duration were observed for the parent $CpMn(CO)_3^+$. Oscillations with the same period were identified in the daughter $CpMn(CO)_2^+$ ion signal as well, as a fingerprint of the parent species.

The dynamics of the parent molecule occurs on two coupled electronic excited states (the bound state a and the repulsive state b), whereby the parent molecule loses one CO ligand. The high temporal resolution of the real-time experiments combined with *ab initio* quantum dynamics calculations allowed the disclosure of intrinsic molecular information encoded in the optimal pulse obtained for optimization of the $CpMn(CO)_3^+$ ion yield [133], by explaining the mechanism of the pump–probe measurements. In this way it was demonstrated that the optimization algorithm finds an intelligent way to increase the photo-ionization of $CpMn(CO)_3$. Due to the slightly different wavelength at which the control experiment was performed with respect to the laser wavelength used in the pump–probe measurements, fragmentation into $CpMn(CO)_2$ was avoided.

The adaptive feedback control scheme was applied on $CpMn(CO)_2^+$, the first fragment emerging from $CpMn(CO)_3^+$, too. This was done by exclusively optimizing the phase of the laser pulse. The experiment increased the relative ion yield of the chosen reaction path ($CpMn(CO)_3^+ \rightarrow CpMn(CO)_2^+ + CO$)

by a factor of 1.5. In this case, the free optimization experiment lead to an optimal pulse shape which is complicated and difficult to interpret [134]. The reason might be that in a free optimization the learning algorithm looks for solutions in a large searching space of 128 dimensions.

Reducing the searching space, e.g. by parametric optimization, would help the evolutionary algorithm not only to converge faster, but would also direct him on the right track towards the desired target. A parametric optimization implies the choice of few characteristics of the laser pulse (spectral FWHM, pulse intensity, time duration, chirp of different orders or even generation of two or more pulses and changing their particular parameters and time separations); these parameters are then "improved" by the feedback loop. For example, if the optimization experiment starts with a triple pulse, would it be able to find the same solution displayed in Figure 6.14? Moreover giving the input pulse from Figure 6.14 as an initial guess, would the algorithm converge to the same solution? Accurate power dependent optimizations should also give additional information about the importance of the third subpulse in the optimal pulse sequence obtained for optimizing the photo-ionization process in $CpMn(CO)_3^+$.

Certainly, it is possible that some components of the pulse might not contribute to the effect and are therefore not considered by the optimization, as presented in Ref. [115]. Hence an important step towards understanding the acquired pulses is to reduce the unimportant components of the light field, by adding "genetic pressure" to the cost functional.

In the case of the fragment optimization, the information coded in the optimal pulse obtained for $CpMn(CO)_2^+$ is difficult to "read". Optimization experiments at higher photon energies would help to understand the mechanism of fragmentation from the parent molecule.

It is also of high interest whether the applied optimization method would find always the same optimal pulse sequence for other complex molecules, similar to the one investigated here. An optimal field which consists of three subpulses was repeatedly observed for simple model systems, e.g. alkali metal clusters (see Chapter 8 or Ref. [20]). An interpretation attempt was that the first subpulse excites the molecules, followed at optimal times by a second subpulse, which ionizes the system. The second subpulse is then followed by a third subpulse, which waits another optimal time for an effective ionization. (A two subpulse sequence with optimal time separations would give a trivial explanation in terms of pump–probe experiments.) Other organometallic molecules with low symmetry (preferably C_s) and different fragmentation branches (different types of ligands) would not only give hints if a triple pulse sequence is optimal for photo-ionization control, but because of their numerous dissociation channels they would give insights of how the fragmentation

mechanism occurs.

One-color pump–probe experiments at $\lambda_{pump} = \lambda_{probe} = 805$ nm would verify the selection rule of the excitation mechanism. Because at low molecular beam temperatures (below 10 K) the molecule has C_s symmetry, a single photon at 402.5 nm or non-polarized two-photons at 805 nm pump pulses can populate the same excited states a and b. This experiments are useful for verifying the two-photon excitation performed by the first "pump" sub-pulse of the optimal pulse from Figure 6.14.

Two-color pump–probe experiments at shorter wavelengths would reveal the wave packet dynamics in the bound c state which has an oscillation period of $T_{osc} \sim 170$ fs [121]. Since in this present work it was clearly demonstrated that the investigated system is very sensitive to the employed central wavelengths and pulse peak intensities, the future experiments should take into account these parameters. By keeping the pulse intensities low, on the order of a few GW cm^{-2}, significant Stark shifts can be avoided. By keeping the pulse durations to 40 fs or less, the ultrafast vibrational dynamics which take place in this molecule can be clearly resolved.